

Structural Basis for the Activity of Drugs that Inhibit Phosphodiesterases

Graeme L. Card,¹ Bruce P. England,¹
Yoshihisa Suzuki,¹ Daniel Fong,¹ Ben Powell,¹
Byunghun Lee,¹ Catherine Luu,¹
Maryam Tabrizizad,¹ Sam Gillette,¹
Prabha N. Ibrahim,¹ Dean R. Artis,¹ Gideon Bollag,¹
Michael V. Milburn,¹ Sung-Hou Kim,²
Joseph Schlessinger,³ and Kam Y.J. Zhang^{1,*}

¹Plexxikon, Inc.

91 Bolivar Drive
Berkeley, California 94710

²Department of Chemistry
University of California, Berkeley
Berkeley, California 94720

³Department of Pharmacology
Yale University School of Medicine
333 Cedar Street
New Haven, Connecticut 06520

Summary

Phosphodiesterases (PDEs) comprise a large family of enzymes that catalyze the hydrolysis of cAMP or cGMP and are implicated in various diseases. We describe the high-resolution crystal structures of the catalytic domains of PDE4B, PDE4D, and PDE5A with ten different inhibitors, including the drug candidates cilomilast and roflumilast, for respiratory diseases. These cocrystal structures reveal a common scheme of inhibitor binding to the PDEs: (i) a hydrophobic clamp formed by highly conserved hydrophobic residues that sandwich the inhibitor in the active site; (ii) hydrogen bonding to an invariant glutamine that controls the orientation of inhibitor binding. A scaffold can be readily identified for any given inhibitor based on the formation of these two types of conserved interactions. These structural insights will enable the design of isoform-selective inhibitors with improved binding affinity and should facilitate the discovery of more potent and selective PDE inhibitors for the treatment of a variety of diseases.

Introduction

Phosphodiesterases (PDEs) play a critical role in maintaining the cellular level of cyclic adenosine monophosphate (cAMP) and cyclic guanosine monophosphate (cGMP) (Beavo, 1995; Conti and Jin, 1999; Houslay, 1998). cAMP and cGMP are ubiquitous second messengers that mediate biological responses to a variety of extracellular cues, including hormones, neurotransmitters, chemokines, and cytokines. Increased concentration of these cyclic nucleotides results in the activation of protein kinase A and protein kinase G. These protein kinases phosphorylate a variety of substrates, including transcription factors and ion channels, which regulate

a myriad of physiological processes, such as immune responses, cardiac and smooth muscle contraction, visual response, glycogenolysis, platelet aggregation, ion channel conductance, apoptosis, and growth control (Francis et al., 2001). Cellular levels of cAMP and cGMP are regulated by the relative activities of adenylyl and guanylyl cyclases, which synthesize these cyclic nucleotides, and by PDEs, which hydrolyze them into 5'-nucleotide monophosphates. By blocking phosphodiester hydrolysis, PDE inhibition results in higher levels of cyclic nucleotides. Therefore, PDE inhibitors may have considerable therapeutic utility as anti-inflammatory agents, antiasthmatics, vasodilators, smooth muscle relaxants, cardiostimulants, antidepressants, antithrombotics, and agents for improving memory and other cognitive functions (Corbin and Francis, 2002; Rotella, 2002; Souness et al., 2000).

Of the 11 classes of human cyclic nucleotide phosphodiesterases, the PDE4 family of enzymes is selective for cAMP, while the PDE5 enzyme is selective for cGMP (Beavo and Brunton, 2002; Conti, 2000; Mehats et al., 2002). Within the PDE4 subfamily, which is comprised of four members (Houslay and Adams, 2003), PDE4B is of particular importance in the inflammatory responses of lymphocytes. Indeed, targeted disruption of the PDE4B gene resulted in viable mice (Jin and Conti, 2002). However, monocytes isolated from these mice exhibit dramatically reduced cytokine production in response to lipopolysaccharide (Jin and Conti, 2002). Hence, PDE4B represents an attractive target for anti-inflammatory therapeutics, and a number of PDE4 inhibitors are currently being tested in late stages of clinical development. For example, cilomilast (Ariflo) and roflumilast (Daxas) have been applied for the treatment of asthma and chronic obstructive pulmonary disease (COPD) with very encouraging results (Barnette et al., 1998; Bundschuh et al., 2001; Hatzelmann and Schudt, 2001). However, it is thought that nausea and emesis, the most common side effects of PDE4 inhibitors, are caused by the inhibition of PDE4D in the brain (Robichaud et al., 2002). Design of inhibitors selective toward different PDE4 subtypes is challenging due to the high degree of sequence and structural similarity. Understanding of these PDE4 subtypes at the atomic level would greatly facilitate the design of subtype-selective inhibitors with reduced side effects and improved pharmacological profiles.

The PDE5 isoform is expressed in smooth muscle tissue, importantly, in the *corpus cavernosum* (Corbin and Francis, 1999). The PDE5 inhibitor sildenafil (Viagra) provides an effective treatment for erectile dysfunction (Ballard et al., 1998) since this drug enhances the level of cGMP activity that accompanies sexual arousal. Vardenafil (Levitra) (Haning et al., 2002) and tadalafil (Cialis) (Porst, 2002) are two additional PDE5 inhibitors that have recently been approved for the treatment of erectile dysfunction. Despite the clear utility of these compounds, one potential drawback is cross-reactivity with the closely related PDE6 and PDE11. It is thought that

*Correspondence: kzhang@plexxikon.com

Table 1. Residues Lining the Active Site of PDE4B, PDE4D, and PDE5A Are Divided into Three Pockets

Function	Symbol	PDE4B	PDE4D	PDE5A
Metal binding pocket	M	H234, H238, H274, D275, H278, N283, L303, E304, D346, M347, D392	H160, H164, H200, D201, H204, N209, L229, E230, D272, M273, D318	H613, H617, H653, D654, H657, N662, M681, E682, D724, L725, D764
Q switch and P clamp pocket	Q	Y233, L393, N395, P396, Y403, W406, T407, I410, M411, M431, V439, S442, Q443, F446	Y159, L319, N321, P322, Y329, W332, T333, I336, M337, M357, V365, S368, Q369, F372	Y612, L765, A767, I768, Q775, I778, A779, V782, A783, L804, I813, M816, Q817, F820
Solvent-filled side pocket	S	G280, S282, E413, F414, <u>Q417</u>, S429, C432	G206, S208, E339, F340, <u>Q343</u>, S355, C358	G659, N661, E785, F786, <u>Q789</u>, T802, M805

Residues in bold are absolutely conserved in all PDEs. Residues that are underlined are conserved in both cAMP- and cGMP-specific PDEs.

this cross-reactivity is responsible for side effects such as blue-tinged vision and back and muscle pain that were experienced by some patients that were treated with these drugs (Gresser and Gleiter, 2002). The availability of PDE5 structural information may enable the development of new PDE5 inhibitors with improved selectivity toward PDE5 versus PDE6 and PDE11.

Our understanding of the mode of action and function of PDEs has been greatly enriched through the crystal structures of the catalytic domains of PDE1B (Zhang et al., 2004), PDE3B (Scapin et al., 2004), PDE4B (Xu et al., 2000, 2004; Zhang et al., 2004), PDE4D (Huai et al., 2003a, 2003b, 2003c; Lee et al., 2002; Zhang et al., 2004), PDE5A (Huai et al., 2003b; Sung et al., 2003; Zhang et al., 2004), and PDE9A (Huai et al., 2004). However, these structures do not shed light on the key interactions that define the common and selective features of the various inhibitors. We report here the cocrystal structures of PDE4B, PDE4D, and PDE5A chimera in complex with ten known inhibitors, including several drug candidates at late-stage clinical development. These cocrystal structures have revealed two common features of inhibitor binding to PDEs: a planar ring structure of the inhibitor that is held tightly in the active site by a pair of hydrophobic residues, and hydrogen bond (H bond) interactions with an invariant glutamine residue that is essential for nucleotide recognition and selectivity (Zhang et al., 2004). These two common features define the scaffold of all known PDE inhibitors. We found that interactions with residues lining the two hydrophobic pockets near the invariant purine-selective glutamine are important for inhibitor binding. The inhibitor potency can be further increased by exploring interactions with residues near the dimetal ion center as well as through the formation of water-mediated interactions with the metal ions. We also demonstrate that the selectivity of inhibitors toward different members of the PDE family can be achieved by exploiting the differences in the shape and hydrophobicity of the binding pockets near the invariant purine-selective glutamine.

Results and Discussion

The Inhibitor Binding Site of PDEs

The cocrystal structures of the catalytic cores of PDE4B, PDE4D, and PDE5A, in complex with different inhibitors

bound to the active site, revealed an overall topology of a compact α -helical structure consisting of three subdomains (Huai et al., 2003a, 2003b, 2003c; Lee et al., 2002; Sung et al., 2003; Xu et al., 2000). The PDE active site forms a deep pocket located at the junction of the three subdomains and is lined with highly conserved residues (Table 1). The active site is approximately 15 Å deep and has an opening of approximately 20 Å by 10 Å (Figure 1A). At the wider side of the active site is a binuclear metal ion center. Both metal ions adopt near-ideal octahedral coordination geometry. The first metal ion is a zinc ion (Zn^{2+}) that is coordinated by two histidines, two aspartates, and two water molecules. These two histidines and two aspartates are absolutely conserved across all the PDE family members. The second metal ion is most probably a magnesium ion (Mg^{2+}) that is coordinated by the same aspartate that also coordinates to Zn^{2+} , and five water molecules, one of which bridges the Mg^{2+} and Zn^{2+} . At the narrow side of the pocket are the invariant purine-selective glutamine and a pair of conserved residues that form the hydrophobic clamp (herein referred to as P clamp). The active site pocket has a surface area of approximately 671 Å², 677 Å², and 675 Å² and a volume of 875 Å³, 925 Å³, and 927 Å³ in PDE4B, PDE4D, and PDE5A, respectively.

The active site can be subdivided into three pockets (Figure 1A): a metal binding pocket (M pocket); a solvent-filled side pocket (S pocket); and a pocket containing the purine-selective glutamine and hydrophobic clamp (Q pocket). The M pocket contains the dimetal ions and highly conserved hydrophobic and polar residues that coordinate the metal ions (Figure 1A and Table 1). The S pocket consists mainly of hydrophilic amino acids and is filled with a network of water molecules in most of the inhibitor complexes. This region is mostly conserved among PDE4B and PDE5A (Table 1).

The Q pocket can be further divided into three distinct areas: a "saddle" formed by the conserved glutamine and the P clamp, flanked by two narrow but deep hydrophobic pockets (Q_1 and Q_2) (Figures 1B and 1C). This region is comprised mainly of hydrophobic residues that are less conserved than the residues of the M pocket (Figure 1D; Table 1), with $Q443^{4B}$ and $N395^{4B}$ being particularly important for nucleotide recognition (where the superscript identifies the protein to which the residue belongs, i.e., 4D for PDE4D, 4B for PDE4B, and 5A for

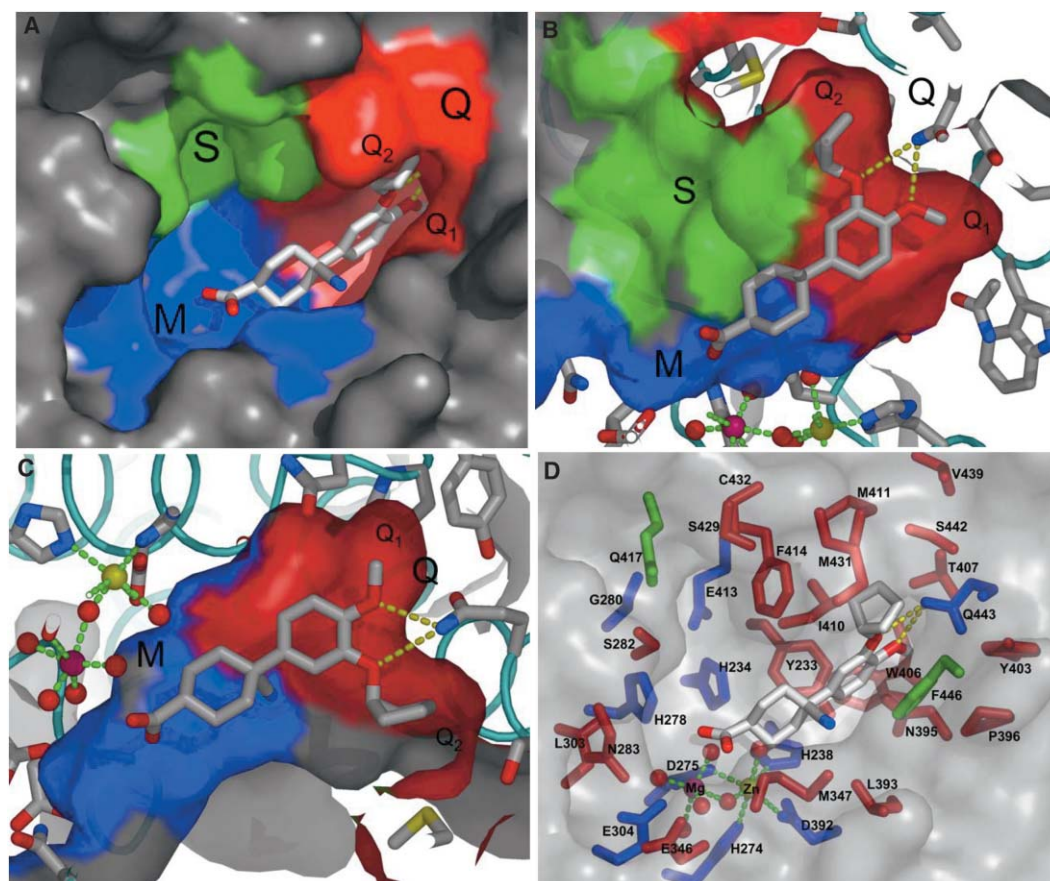


Figure 1. Classification of the Active Site of PDEs

(A) The active site of PDEs is divided into three pockets: the metal binding pocket (M) shown in blue, the purine-selective glutamine and hydrophobic clamp pocket (Q) shown in red (which is further divided into Q₁ and Q₂ subpockets), and the solvent-filled side pocket (S) shown in green. This color coding of the active site pocket is mapped on the surface of PDE4B in complex with cilomilast, which is shown as a stick model bound at the active site. The cocrystal structure of PDE4B in complex with cilomilast has also been used to display the surfaces in (B)–(D).

(B) Same as (A), but a view of the PDE active site looking toward the S pocket. This view is a clockwise rotation of about 90° along the length of cilomilast from the view in Figure 1A. The subpockets that subdivide the Q pocket are also labeled: Q₁ is the small subpocket, and Q₂ is the large subpocket.

(C) Same as (A), but a view of the PDE active site looking away from the S pocket. This view is a counterclockwise rotation of about 90° along the length of cilomilast from the view in Figure 1A. All the subpockets are labeled.

(D) Residues lining the three active site pockets. The active site surface is semitransparent to reveal residues that make up the active site. The absolutely conserved residues in all PDEs are colored blue. Residues conserved in both cAMP- and cGMP-specific PDEs are colored green. The other variable residues are colored red.

the chimeric PDE5A. This naming convention will be used hereafter.). The Q₁ pocket is a small hydrophobic pocket pointing away from the S pocket, while the Q₂ pocket is larger and adjacent to the S pocket. Because of the less conserved nature of the residues in the Q pocket of different PDE family members, these regions may be exploited for generating isoform-selective PDE inhibitors.

Defining the Scaffold

The superposition of all the inhibitors bound to PDE4D, PDE4B, and PDE5A has revealed with astounding clarity that there is a highly conserved binding mode among all the inhibitors of drastically different chemotypes (Figures 2A–2D). All these inhibitors share a core binding site distal to the dimetal ions that can be characterized

by a planar ring sandwiched by the hydrophobic clamp and the formation of an H bond with an invariant glutamine. The substructure of the inhibitors that bind to this core represents a framework upon which more potent and selective inhibitors can be developed.

All the known inhibitors bound to PDEs occupy part of the active site, primarily around the Q pocket and occasionally close to the M pocket (Figure 2B). The interactions that these inhibitors make with PDE4B, PDE4D, and PDE5A can be split into three major types: interactions with the metal ions mediated through water; H bond interactions with the protein residues involved in nucleotide recognition; and most importantly, the interaction with the hydrophobic residues lining the cavity of the active site. These three types of interactions have evolved to bind the natural substrate, as displayed in

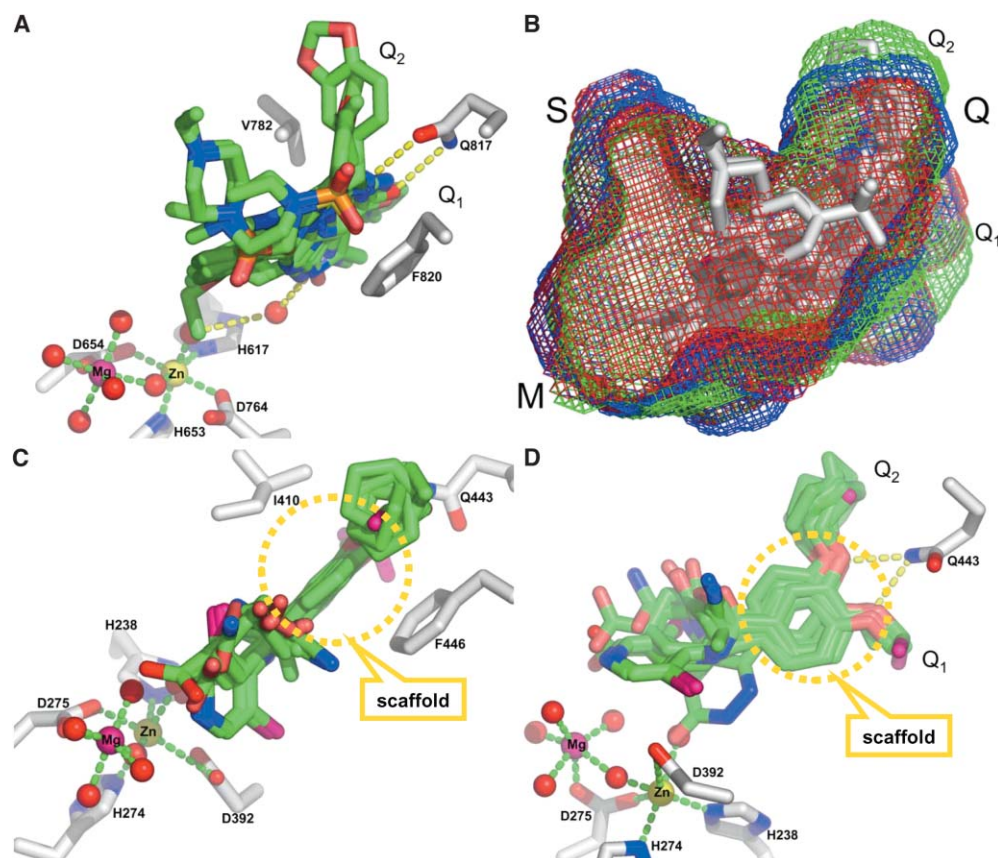


Figure 2. Common Features of Inhibitor Binding to PDEs Define the Scaffold

(A) Superposition of the structures of sildenafil and vardenafil in complex with PDE4B and PDE5A as well as tadalafil bound to PDE5A has shown that the hydrophobic clamp and H bond with purine-selective glutamine are highly conserved. The protein side chain atoms are represented by default atomic colors (oxygen shown in red, nitrogen shown in blue, sulfur shown in yellow), except the carbon atom is represented by gray. The zinc ion is shown in yellow, the magnesium ion is shown in magenta, and phosphorus is shown in purple. The compound atoms are also represented accordingly by using default atomic colors, with the exception of carbon, which is represented by various colors for different compounds for easy distinction. The color coding scheme is followed for all the figures when possible.

(B) Solvent-accessible surface areas in the active sites of PDEs. All the known inhibitors bound to PDE4B, PDE4D, and PDE5A occupy part of the active site pocket primarily around the Q pocket and sometimes close to the M pocket. The red, blue, and green meshes represent the solvent-accessible surface area of the active site pocket in PDE4B, PDE4D, and PDE5A, respectively. All the inhibitors are represented by gray sticks. Note that the Q₂ pocket of PDE5A is significantly larger than that of PDE4B and PDE4D, and tadalafil pokes deep into this pocket.

(C) Superposition of the structures of all the dialkoxyphenyl compounds bound to PDE4B and PDE4D. The phenyl rings superimpose well and are sandwiched in between the hydrophobic clamp, F446^{4B}, and I410^{4B}. The substituents have more diverse conformations that exploit the large M pocket to attain various binding affinities.

(D) Same as (C), but a view at about 90° rotation along the length of the molecule to reveal the conserved binding of the catechol scaffold. The phenyl ring and the two alkoxy groups superimposed very well in all ten cocrystal structures.

the cocrystal structures of PDE4B, PDE4D, and PDE5A, with AMP and GMP (Zhang et al., 2004). All known inhibitors seem to exploit these three types of interactions, and hence these interactions should guide the design of new types of inhibitors.

The major contributor to inhibitor binding involves hydrophobic interactions with residues lining the active site pocket that are listed in Table 1. A key feature of these hydrophobic interactions and a common binding mode to all of these inhibitors is a “hydrophobic clamp” that anchors these inhibitors in the active site. This P clamp consists of a pair of highly conserved hydrophobic residues, in which one jaw of the clamp is a phenylalanine in all PDE family members (F446^{4B}, F372^{4D}, F820^{5A}), except in PDE11, in which the corresponding residue is

W428^{11A}. A variable, but always hydrophobic, residue forms the opposite jaw of the clamp and is a valine, leucine, or isoleucine in all of the PDEs, e.g., I410^{4B}, I336^{4D}, and V782^{5A}. In virtually all of the inhibitor structures, the structural elements of the P clamp are conserved and focused on the aromatic ring of the inhibitors presenting the hydrogen bonding residues to the invariant glutamine. The phenylalanine engages this primary aromatic ring of the inhibitor from above with an offset face-on-face interaction (Burley and Petsko, 1985), while the γ -carbon of the β -branched residue below is centered under the same ring. In the catecholdiether-containing inhibitors, the face-on-face interaction centers the carbon bearing the meta-alkoxy substituent under the phenylalanine, while, in sildenafil and similar ana-

logs, the polarized biaryl-linked carbon of the bicyclic aromatic group occupies a similar position. The substituents at these two types of positions thus serve a dual role, both to optimize local hydrophobic interactions with the enzymes, and to modulate the position and polarity of the P clamp. This subtle variation affords some of the inhibitors their selectivity over different PDE family members. However, the sequence variation among additional residues lining the hydrophobic pocket affords greater selectivity to the inhibitor. Interestingly, given the bicyclic nature of the cAMP and cGMP substrates, all of the hydrophobic interactions appear to be focused on the primary aromatic ring. In the cases of the inhibitors containing a bicyclic core, the second (fused) ring predominantly contributes productive hydrophobic interactions through the presentation of various substituents.

The residues involved in nucleotide recognition make up a secondary yet important component in inhibitor binding and also enable specificity toward different PDE families. The invariant glutamine residue (Q443^{4B}, Q369^{4D}, and Q817^{5A}), which switches its orientation for the recognition of cAMP or cGMP ("Q switch") (Zhang et al., 2004), is always H bonded to the inhibitors described here and it is either a single or a bidentate H bond. Since the orientation of the γ -amide group of this invariant glutamine is anchored through an intricate network of H bonds with nearby residues, this invariant glutamine residue also plays a role in the control of specificity toward different inhibitors. For example, both sildenafil and vardenafil form two H bonds with Q817^{5A}, but they only form one H bond with Q443^{4B}. This is because the pyrazolopyrimidinone group of sildenafil mimics guanine and contributes the same H bond donor and acceptor features as guanine in forming a bidentate H bond with Q817^{5A} with its amide orientation evolved to bind cGMP. However, this H bond donor and acceptor feature of the pyrazolopyrimidinone group in sildenafil is unable to form bidentate H bonds with Q443^{4B}; thus, a single H bond results. This provides a partial explanation for the specificity of sildenafil for PDE5A over PDE4B/4D.

Optimizing Inhibitor Potency

Analysis of the cocrystal structures of the dialkoxyphenyl compounds bound to PDE4B and PDE4D has revealed that an important way for increasing inhibitor potency is to design substituents to the scaffold that could pick up hydrophobic interactions with residues in the M pocket and also create water-mediated interactions with the metal ions. These cocrystal structures have also shown that the hydrophobic interactions with residues lining the Q₁ and Q₂ pockets are very important for inhibitor potency.

The superposition of our cocrystal structures of this dialkoxyphenyl family of compounds with PDE4B and PDE4D reveals that the scaffold is a catechol that makes the H bond with the purine-selective glutamine and is also sandwiched by the P clamp (Figures 2C and 2D). The catechol scaffold superposed extremely well in all of the 11 structures of the 7 compounds, whereas the substituents showed significant variations in their binding conformation as well as in the residues that they

interact with. The catechol group interacts with the residues that have evolved for purine binding, whereas the substituents on the phenyl ring are exploring the site for the ribose moiety of cAMP and to some extent reaching the phosphate binding site. The dialkoxyphenyl family of compounds almost all contain one carbon ether, e.g., methoxy or difluoromethoxy, and a cyclic multicarbon ether, e.g., cyclopentyloxy or cyclopropylmethyl. The smaller methoxy or difluoromethoxy group on the phenyl ring is tucked into a small pocket at the deep side of the Q₁ pocket formed by Y233^{4B}, N395^{4B}, T407^{4B}, and Y403^{4B} (Table 1). The other alkoxy group tends to be a larger hydrophobic group such as cyclopentyl, propyl, or cyclopropyl methyl. They occupy a larger hydrophobic Q₂ pocket formed by F414^{4B}, M411^{4B}, M431^{4B}, and F446^{4B} (Table 1).

The dialkoxyphenyl compounds described are all substituted at the para-position to a methoxy or difluoromethoxy group. Zardaverine (Schudt et al., 1991) is the only exception in that it has a substitution at the meta-position to the methoxy group. Although the asymmetry of most of the dialkoxyphenyl compounds matches with the size of the Q₁ and Q₂ pocket and hence determines the unique orientation of the catechol scaffold binding, the relatively smaller difluoromethoxy group in zardaverine could also fit into the Q₁ pocket as an alternative to the methoxy group. Consequently, two major binding modes have been observed in our 1.54 Å resolution cocrystal structure (Figures 3A and 4A). One of the binding modes has the difluoromethoxy group binding at the Q₁ pocket and, subsequently, the pyridazinone substituent pointing away from the dimetal ions (yellow molecule in Figure 3A). This is similar to the binding mode of zardaverine to PDE4D in the 2.9 Å resolution cocrystal structure reported by Lee et al. (2002). This binding mode only accounts for about 20% of the zardaverine in our structure. The predominant binding mode is with the methoxy group binding to the Q₁ pocket and the difluoromethoxy group binding to the Q₂ pocket. As a result, the pyridazinone substituent points toward the dimetal ions and forms a direct coordination with the Zn²⁺ by displacing one of its bound water molecules (Figure 4A). Surprisingly, this predominant binding mode of zardaverine was not observed in the cocrystal structure of zardaverine with PDE4D reported by Lee et al. (2002). However, they have observed the binding of an arsenate ion near the dimetal ions in the active site. The presence of this arsenate ion might have prevented zardaverine from binding in the predominant mode. Since the two heterocyclic nitrogens in the pyridazinone ring are not anchored by H bonds to the protein residues, this pyridazinone ring also has two rotational conformations observed in our cocrystal structure (green and cyan molecules in Figure 3A) with occupancy of 47% and 33%, respectively. Thus, we observed a total of three alternate conformations of zardaverine bound to PDE4D.

The various substituents on the dialkoxyphenyl scaffold explore the deep pocket close to the metal binding site, and how well they form interactions with residues lining this pocket determines their relative binding affinity. The relatively smaller pyrrolidinone substituent in rolipram has resulted in a relatively lower binding affinity

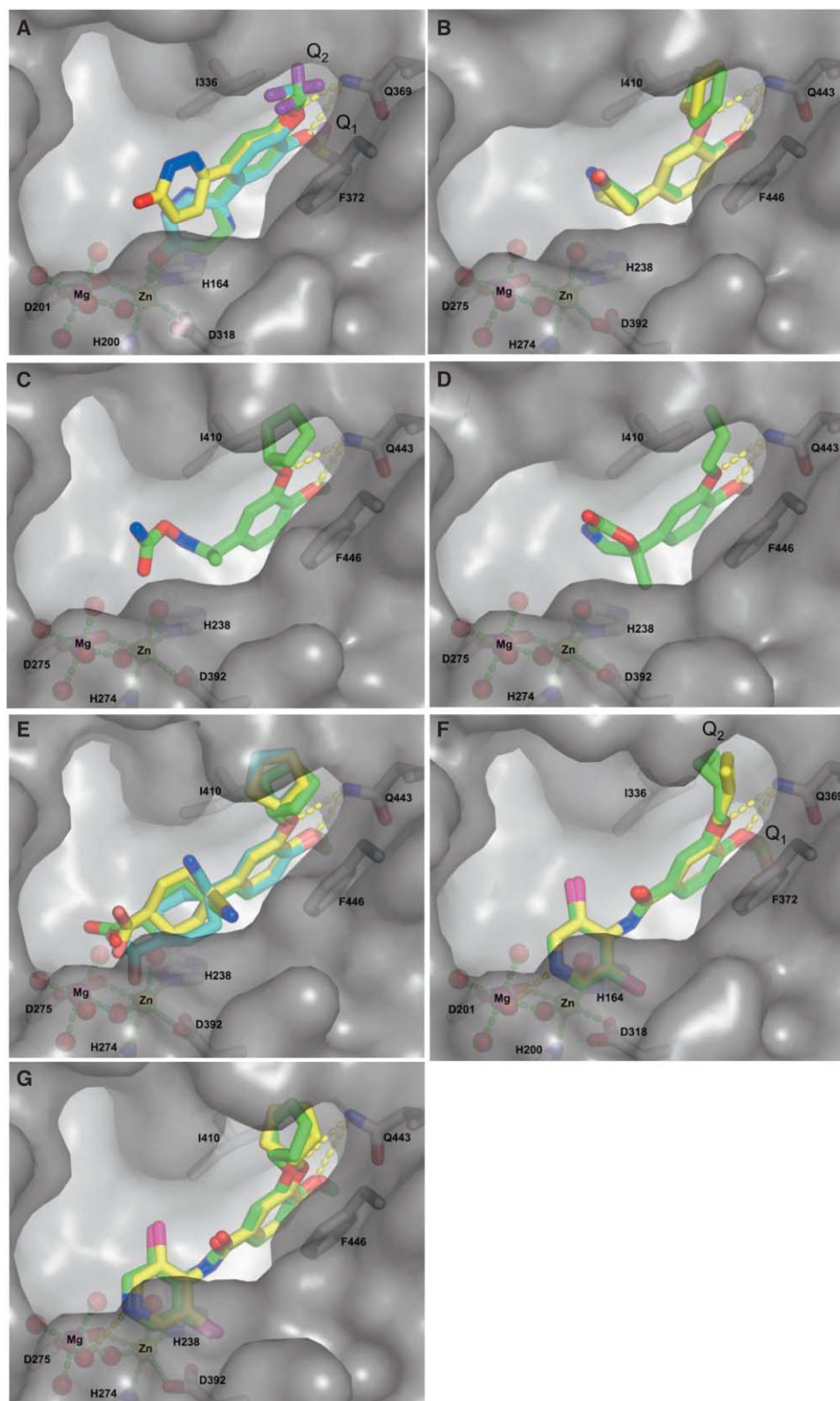


Figure 3. The Cocystal Structures of PDE4B and PDE4D in Complex with the Dialkoxyphenyl Family of Inhibitors

(A) Structure of zardaverine bound to PDE4D. A semitransparent surface of the target protein is overlaid for Figures 3A–3G and also for Figures 5A and 5B. Three alternative conformations of zardaverine have been observed, and their carbon atoms are colored in green, cyan, and yellow, respectively. The predominant conformations that have their difluoromethoxy group pointing up to the Q₂ pocket and their pyridazinone group pointing to the dimetal ions and coordinated to Zn²⁺ by displacing the bound water molecule are represented by green and cyan,

(570 nM in the case of PDE4B). Rolipram exhibits both a low-affinity (350–400 nM) and a high-affinity (5–10 nM) binding state to the full-length PDE4 (Rocque et al., 1997). This could reflect two distinctive conformational states of the catalytic domain that are switched by modifications, such as phosphorylation or interactions with other proteins in the regulatory domains of the PDE4 (Alvarez et al., 1995; Bolger et al., 2003; Houslay and Adams, 2003; McPhee et al., 1999). Our cocrystal of the PDE4 catalytic domain probably has rolipram bound in the low-affinity state, since the 50% inhibition concentration (IC₅₀) values for the rolipram binding to the catalytic domains of PDE4B and PDE4D are 0.57 μ M and 1.1 μ M, respectively (Table 2). In our cocrystal structures of rolipram with PDE4B using either a racemic mixture of (R,S)-rolipram or the R-enantiomer alone, only one binding mode—with the pyrrolidinone group pointing away from the dimetal ions—has been observed (Figures 3B, 4B, and 4C). The same binding mode has also been observed in the 1.6 Å cocrystal structure of rolipram with PDE4D, where a racemic mixture of (R,S)-rolipram has been used in the cocrystallization (Zhang et al., 2004). The pyrrolidinone group is stabilized mainly through hydrophobic interactions with M347^{4B}, I410^{4B}, and F414^{4B}. The rolipram binding mode observed in our cocrystal structures is similar to that observed by Huai et al. (2003c) and different from that reported by Xu et al. (2004), who reported that two binding modes—with the pyrrolidinone group either pointing away from or pointing toward the dimetal ions—have been observed. These differences in rolipram binding could be caused by different crystallization conditions, such as the use of cacodylate in the crystallization medium or soaking versus cocrystallization. However, these two binding modes may reflect alternative conformational states that could be switched by some external factors, such as phosphorylation or protein binding (Alvarez et al., 1995; Bolger et al., 2003; Houslay and Adams, 2003; McPhee et al., 1999). In this regard, the unique ability of certain PDE4 inhibitors, such as rolipram, but not certain other inhibitors, to elicit conformational effects at the surface of the PDE4A4 isoform may reflect their ability to adopt two distinctive binding modes (Terry et al., 2003).

The more potent dialkoxyphenyl compounds have larger substituents that could form more favorable interactions with residues lining the relatively large M pocket.

The hydroxamate and cyclic carbamate substituents of filaminast and mesopram form a similar number of interactions with residues in the M pocket as those of rolipram and zardaverine and therefore have similar binding affinities, of 960 nM and 420 nM, respectively, to PDE4B (Figures 3C and 3D). As the substituents become larger, and exploit more interactions with residues in the M pocket, the potency of the compounds is also increased. The carboxycyclohexyl substituent of cilomilast forms several more interactions with residues in the M pocket compared to the substituents in filaminast and mesopram, and, therefore, cilomilast is a more potent inhibitor exhibiting an IC₅₀ of 25 nM and 11 nM toward PDE4B and PDE4D, respectively (Figure 3E). The cyclohexyl group forms hydrophobic interactions with M347^{4B}, L393^{4B}, and F414^{4B}, while the oxygens of carboxylate form two H bonds with water molecules coordinated to the Mg²⁺. The observed conformational variability of the carboxycyclohexyl group (Figure 3E) may have reduced the binding affinity of cilomilast.

Roflumilast binds similarly to cilomilast (Figure 3F). The difluoromethoxy group binds at the Q₁ pocket, while the cyclopropyl methoxy group binds at the Q₂ pocket. The difluoromethoxy group fits the Q₁ pocket better and makes more hydrophobic interactions with residues lining this pocket than the methoxy group. However, the cyclopropylmethylether group makes fewer hydrophobic interactions than the larger cyclopentylether group. The dichloropyridyl group extends to the dimetal ion site and forms one H bond to a water molecule that is coordinated to Mg²⁺. The dichloro atoms also form additional hydrophobic interactions with residues in the M pocket. The dichloropyridyl substitution has compensated for the negative effect of the cyclopropylmethylether group and as a result has increased the potency of roflumilast by about 30-fold (IC₅₀ = 0.84 nM) as compared to the potency of cilomilast toward PDE4B (Table 2).

Piclamilast can be considered as a hybrid compound, derived from the functionalities in the opposite sides of cilomilast and roflumilast (Figure 3G). The methoxy group binds at the Q₁ pocket, while the cyclopentylether group binds at the Q₂ pocket. These two substituents are the most common in the dialkoxyphenyl compounds, and they seem to be optimized for maximum interactions with residues in the Q₁ and Q₂ pockets. The dichloropyri-

respectively. The minor conformation is represented by yellow and has its difluoromethoxy group pointing down to the Q₁ pocket and its pyridazinone group pointing away from the dimetal ions.

(B) Structure of rolipram bound to PDE4B: cocrystal structures with either (R,S)-rolipram (green) or (R)-rolipram (yellow). Only one binding mode—with the pyrrolidinone group pointing away from the dimetal ions—has been observed. Either enantiomer could fit the electron density (Figure 4B) for the ligand in the (R,S)-rolipram cocrystal structure. The single binding mode observed in this structure does not, therefore, necessarily infer selective cocrystallization of one enantiomer.

(C) Structure of filaminast bound to PDE4B. The hydroxamate substituent extends to the M pocket and is tilted slightly up toward the opening of the pocket.

(D) Structure of mesopram bound to PDE4B. The cyclic carbamate substituent extends to the M pocket and is tilted slightly up toward the opening of the pocket. Although a racemic mixture was used for the cocrystallization, the (R)-mesopram was selectively bound to PDE4B.

(E) Structure of cilomilast bound to PDE4B and PDE4D. The carboxycyclohexyl group adopts two different conformations in the PDE4D complex. The carbon atoms of cilomilast in PDE4B are shown in green, and the carbons of cilomilast in PDE4D are shown in yellow and cyan.

(F) Structure of roflumilast bound to PDE4B and PDE4D. The carbon atoms of roflumilast in PDE4B are shown in green, and the carbons of roflumilast in PDE4D are shown in yellow. The difluoromethoxy group binds at the Q₁ pocket, while the cyclopropyl methyl group binds at the Q₂ pocket. The dichloropyridyl group extends to the dimetal ion site and forms one H bond to a water molecule that is coordinated to Mg²⁺.

(G) Structure of piclamilast bound to PDE4B and PDE4D. The carbon atoms of piclamilast in PDE4B are shown in green, and the carbons of piclamilast in PDE4D are shown in yellow.

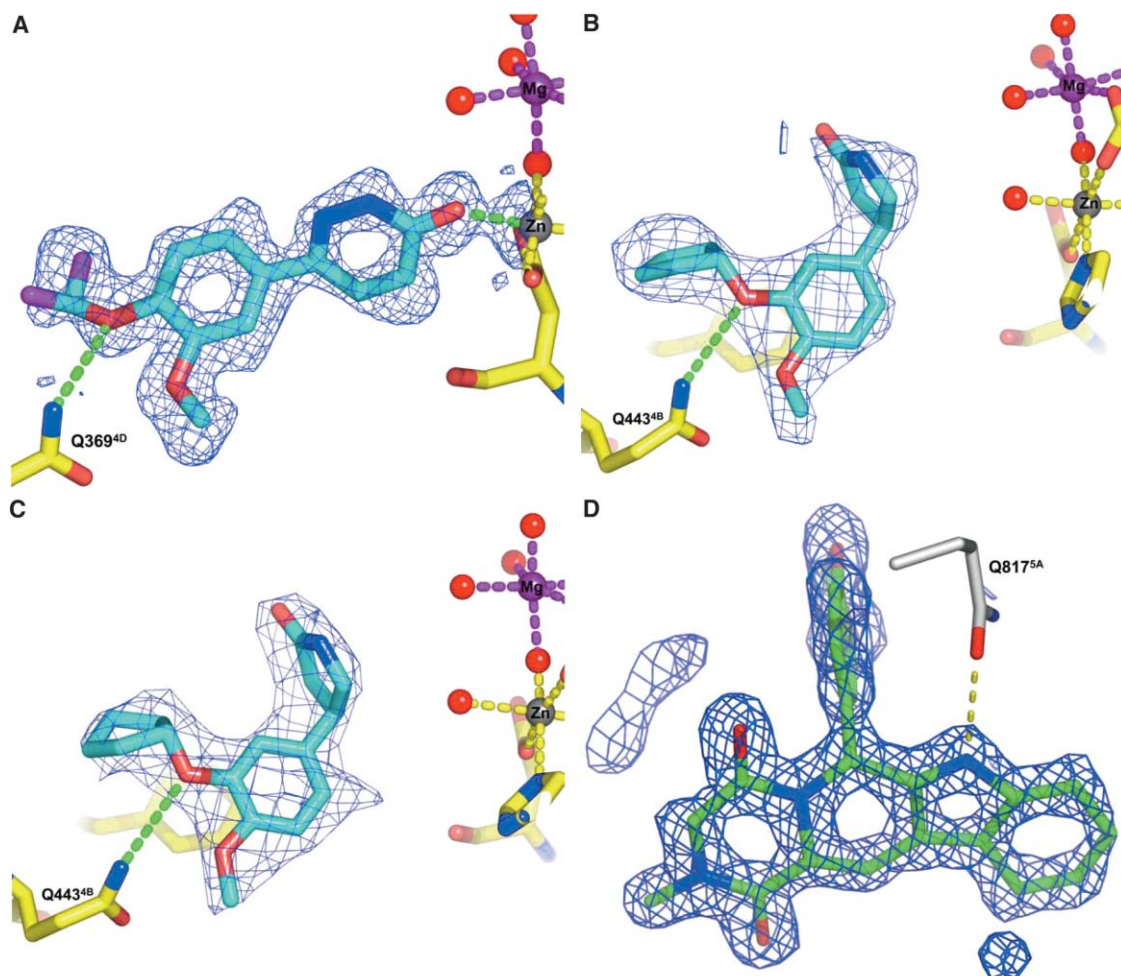


Figure 4. Electron Densities of Inhibitors Bound to PDE4B, PDE4D, or PDE5A

(A) Unbiased electron density that corresponds to zardaverine bound to PDE4D at 1.54 Å. The Fo-Fc electron density is calculated with the phases from the initial model of the PDE4D apo structure after molecular replacement and is therefore unbiased toward the bound ligand. The difference density is contoured at 3 σ and with the stick model of the refined zardaverine superimposed. It shows clearly that zardaverine, in its primary binding mode, is coordinated to the Zn²⁺. The electron density corresponding to the secondary binding mode (at about 20% occupancy) is only revealed after further refinement of the protein as well as zardaverine built into the primary binding mode.

(B) Unbiased electron density that corresponds to (R,S)-rolipram bound to PDE4B at 2.31 Å. The Fo-Fc difference density is contoured at 3 σ . Both enantiomers could fit into the density, and only the (R)-enantiomer is shown as a stick model and overlaid with the electron density. The pyrrolidinone group is pointing away from the dimetal ions with the (R)- or (S)-rolipram binding to PDE4B.

(C) Unbiased electron density that corresponds to (R)-rolipram bound to PDE4B at 2.40 Å. The Fo-Fc difference density is contoured at 3 σ . The stick model of (R)-rolipram is overlaid with the electron density. The electron density is very similar to that in (B) and suggests that the pyrrolidinone group in (R)-rolipram is pointing away from the dimetal ions.

(D) Unbiased electron density that corresponds to tadalafil bound to PDE5A at 1.37 Å. The Fo-Fc electron density is calculated with the phases from the initial model of the PDE5A apo structure after molecular replacement and is therefore unbiased toward the bound ligand. The difference density is contoured at 3 σ and with the stick model of tadalafil superposed. The high quality of the electron density reveals the unambiguous binding mode of tadalafil.

dyl substituent of piclamilast forms hydrophobic interactions with M347^{4B}, L393^{4B}, and F414^{4B}, and the heterocyclic nitrogen on the pyridine ring forms an H bond with a water molecule coordinated to the Mg²⁺. Additionally, the nitrogen and oxygen atoms in the amide that links the dichloropyridyl to the dialkoxyphenyl scaffold each form a hydrogen bond with a water molecule. These extensive interactions formed between piclamilast and the residues in the active site make piclamilast one of the most potent molecules in the dialkoxyphenyl compound series with IC₅₀ values of 41 pM and 21 pM toward PDE4B and PDE4D, respectively (Table 2).

Designing Inhibitor Specificity

There are subtle but significant differences in the active sites of PDE4B and PDE5A that could be exploited to achieve subtype selectivity for inhibitors. The opposite orientation of the purine-selective glutamine between PDE4B and PDE5A as well as the differences among residues near the Q₂ pocket have been the major driving force for inhibitor selectivity between these two family members. Sildenafil and vardenafil have adopted completely different binding modes to PDE4B versus PDE5A in order to avoid some unfavorable interactions and consequently have drastically different binding affinities

Table 2. Biochemical Inhibition Data of All the Known Inhibitors against a Full Panel of PDEs

Inhibitor Name	Structure	PDE1B	PDE2A	PDE3B	PDE4B	PDE4D	PDE5A	PDE7B	PDE8A	PDE9A	PDE10A	PDE11A
Zardaverine		>200	>200	1.5	0.93	0.39	81	>200	160	>200	14	140
(R,S)-Rolipram		>200	>200	>200	0.57	1.1	>200	>200	>200	>200	140	>200
Filaminast		190	89	9.4	0.96	1.0	53	0.99	120	>200	27	57
(R,S)-Mesopram		>200	>200	>200	0.42	1.1	>200	>200	>200	>200	63	>200
Cilomilast		87	160	87	0.025	0.011	53	44	7	>200	73	21
Roflumilast		>200	>200	>200	0.00084	0.00068	17	>200	>200	>200	>200	25
Piclamilast		68	54	11	0.000041	0.000021	3.5	8.8	>200	>200	21	1.6
Sildenafil		1.5	35	15	20	14	0.0022	78	>200	5.6	6.8	6.1
Vardenafil		0.3	3.1	0.58	3.8	3.9	0.0010	1.9	57	0.68	0.88	0.24
Tadalafil		50	130	280	9.2	19	0.0012	74	>200	150	19	0.010

The enzymes used are the catalytic domain of human PDEs. The numbers shown in the table are the 50% inhibition concentration (IC₅₀) in μ M.

to these two enzymes (Figure 5 and Table 2). Tadalafil exploits the significant differences in the shape and size of the Q₂ pocket and attains both potency for PDE5A and selectivity against PDE4B. These structural differences could be exploited to achieve subtype selectivity for other inhibitors as well.

Vardenafil exploits the same interactions with residues involved in nucleotide recognition (Zhang et al., 2004). The amide moiety of the imidazolotriazinone group forms a bidentate H bond with the γ -amide group of Q817^{SA} (Figure 5E). The orientation of its γ -amide group is constrained by an intricate network that in-

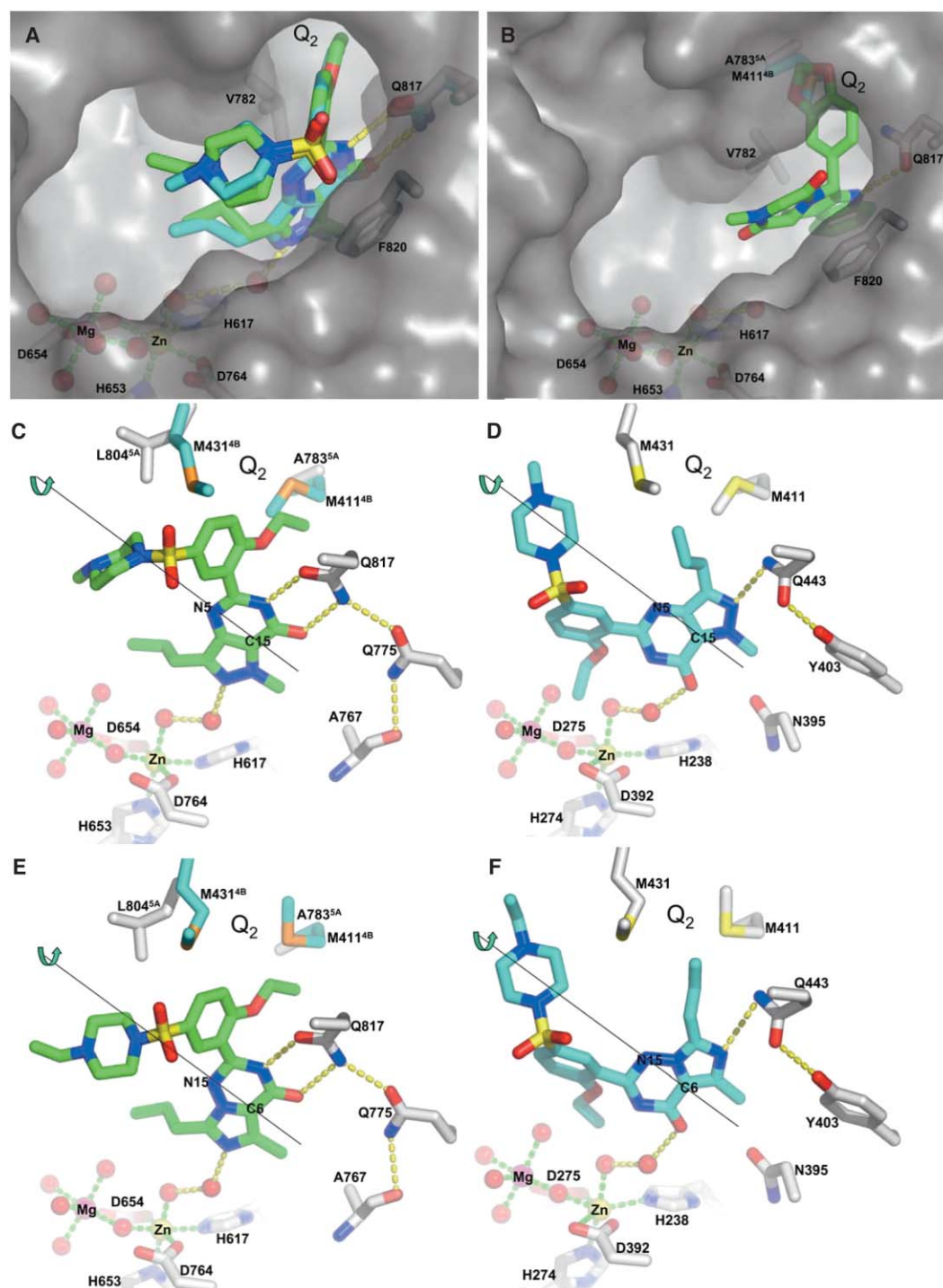


Figure 5. Structures of PDE4B and PDE5A in Complex with Vardenafil, Sildenafil, and Tadalafil

(A) Similar interactions between vardenafil and sildenafil bound to the active site of PDE5A. The carbon atoms of vardenafil are shown in green, and the carbons of sildenafil are represented by cyan. The pyrazolopyrimidinone group in sildenafil and the imidazolotriazinone group in vardenafil both mimic the purine group in the cyclic nucleotide and forms bidentate H bonds with the purine-selective Q817. The heterocyclic nitrogen atom in the pyrazole moiety of sildenafil and the heterocyclic nitrogen atom in the imidazole moiety of vardenafil both form an H bond with a water molecule that is in turn hydrogen bonded to a water molecule coordinating the Zn^{2+} .

(B) Structure of tadalafil bound to PDE5A. Only one H bond has been formed between Q817 and the heterocyclic nitrogen in the indole ring of the pyrazinopyridoindole moiety of tadalafil. The γ -amide group of Q817 rotated about 90° from its orientation in the sildenafil and vardenafil bound structures to accommodate the only H bond donor from tadalafil. The methylenedioxyphenyl group of tadalafil occupies the same hydrophobic pocket (Q_2) as that by the ethoxy group of sildenafil and vardenafil.

(C) Structure of sildenafil bound to PDE5A. The carbon atoms of sildenafil are shown in green. The pyrazolopyrimidinone group in sildenafil mimics the purine group in the cyclic nucleotide and forms bidentate H bonds with the purine-selective Q817. The heterocyclic nitrogen atom

involves H bonding of Q817^{5A} to Q775^{5A} and Q775^{5A} to A767^{5A} as well as W853^{5A}, and it is this constrained orientation that determines nucleotide specificity. The heterocyclic nitrogen of the imidazole moiety forms an H bond with a water molecule that interacts with one of the waters coordinating the Zn²⁺. The hydrophobic interactions are the predominant force in vardenafil binding. Vardenafil has a total surface area of 724 Å², of which 489 Å² is buried by residues within the active site pocket. A large proportion of the surface area (180 Å²) of vardenafil is buried between the P clamp residues V782^{5A} and F820^{5A}, utilizing the π - π stacking interactions of the phenylalanine side chain to that of the imidazolotriazinone moiety (Figure 5A). Additional, more remote hydrophobic contacts to the five-membered ring of the bicyclic core are provided by Y612^{5A} and L765^{5A}. The propyl group from the five-membered ring also forms hydrophobic contacts with L725^{5A} and F786^{5A}. The ethoxyphenyl group makes hydrophobic contacts with V782^{5A}, F786^{5A}, A779^{5A}, I813^{5A}, and M816^{5A}. Vardenafil shows a very similar binding mode to sildenafil (Figure 5A), and the cocrystal structure of sildenafil with PDE5A chimera has been reported (Zhang et al., 2004). The ethylpiperazine group makes similar interactions with PDE5A as the methylpiperazine of sildenafil. The piperazine ring adopts a slightly different orientation that is probably due to the relative dearth of specific interactions between this group and the protein.

Tadalafil binds to PDE5A very differently from sildenafil and vardenafil, due to its different chemical nature (Figures 5B and 4D). The methyne at the bridgehead between the two six-membered rings is the focal point of the P clamp interaction with F820^{5A} and V782^{5A}. In addition to the interactions with the P clamp, the nearly flat four-ring moiety of pyrazinopyridoindole is held in place through hydrophobic interactions with side chains of I768^{5A}, I778^{5A}, F786^{5A}, and L804^{5A}. The indole core is sandwiched between F786^{5A}, L804^{5A}, and F820^{5A}. The methylenedioxyphenyl group of tadalafil occupies the Q₂ pocket (Figure 5B) and makes hydrophobic interactions with A783^{5A}, F786^{5A}, F787^{5A}, L804^{5A}, I813^{5A}, and M816^{5A}. The methylenedioxyphenyl group does not fit into the relatively smaller Q₂ pocket in PDE4B and could

cause steric clashes with M411^{4B} (cf. to A783^{5A}, Figure 5B). This confers tadalafil not only its high potency with PDE5A but also its selectivity against PDE4B. Tadalafil only forms one H bond with Q817^{5A} through its NH group on the indole ring. Consequently, the γ -amide group of Q817^{5A} rotates by 90° from its orientation in the sildenafil bound structure to accommodate the only H bond donor from tadalafil. Thus, the binding mode of tadalafil reveals the only case observed in these structures in which the presentation of the hydrogen bond interaction with the conserved glutamine is made from a different ring system than the one held in the P clamp. This orientation of the γ -amide group of Q817^{5A} determines how Q817^{5A} interacts with the adenine moiety upon cAMP binding. Tadalafil makes neither direct nor water-mediated interactions with the metal ions. Despite the lack of H bonded interactions with the protein, tadalafil makes many hydrophobic interactions that contribute to its high potency. Moreover, the rigid chemical structure of tadalafil with only one nonterminal rotatable bond has also contributed to its high binding affinity since it loses less entropy upon protein binding compared to sildenafil and vardenafil.

Sildenafil and vardenafil display limited potency as inhibitors against PDE4B (IC₅₀ = 20 μ M and 26 μ M, respectively), but their potency is significantly higher for PDE5A (IC₅₀ = 0.0022 μ M and 0.0010 μ M, respectively). The dramatic difference in binding affinity between PDE4B and PDE5A is due to the different binding mode seen in PDE4B versus PDE5A when the cocrystal structures in the presence of sildenafil or vardenafil are compared (Figures 5C–5F). The driving force behind this difference in binding can be attributed to relieving unfavorable electrostatic interactions and steric clashes. These interactions are due to sequence changes between the active site pocket of PDE5A and PDE4B (mainly A783^{5A} to M411^{4B} and L804^{5A} to M431^{4B}), as well as the orientation constraints of Q443^{4B} caused by its unique H bonding pattern, locking the γ -amide group into one orientation. Consequently, there is an almost 180° flip in the orientation along the N5-C15 axis for sildenafil (Figures 5C and 5D) and along the corresponding C6-N15 axis for vardenafil (Figures 5E and 5F). This

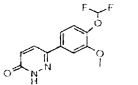
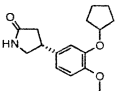
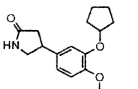
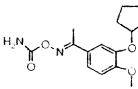
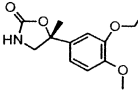
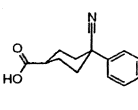
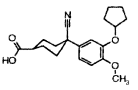
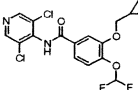
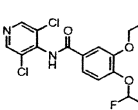
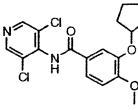
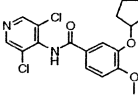
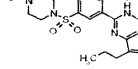
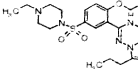
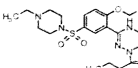
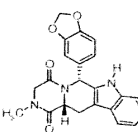
in the pyrazole moiety of sildenafil forms an H bond with a water molecule that is in turn hydrogen bonded to a water molecule coordinating the Zn²⁺. The same binding mode of sildenafil in PDE4B would cause steric clashes with side chains of M431^{4B} and M411^{4B}, shown in cyan, in the Q₂ pocket.

(D) Structure of sildenafil bound to PDE4B. The carbons of sildenafil bound to PDE4B are represented by cyan. In order to avoid the steric clashes with M431 and M411 in the Q₂ pocket and also the incompatible H bonding characteristics of Q443, sildenafil has flipped about 180° along the axis of N5 and C15 from its binding orientation in PDE5A. Consequently, only one H bond was formed between Q443 and the heterocyclic nitrogen in the pyrazole ring. The heterocyclic nitrogen in the pyrazole ring has almost traded places with the heterocyclic nitrogen in the pyrimidinone ring in the sildenafil bound to PDE4B as compared to the sildenafil bound to PDE5A. An H bond is formed between the exocyclic oxygen on the pyrimidinone ring and a water that is coordinated to the Zn²⁺.

(E) Structure of vardenafil bound to PDE5A. The carbon atoms of vardenafil are shown in green. The imidazolotriazinone group in vardenafil mimics the purine group in the cyclic nucleotide and forms bidentate H bonds with the purine-selective Q817. The heterocyclic nitrogen atom in the imidazole moiety of vardenafil forms an H bond with a water molecule that is in turn hydrogen bonded to a water molecule coordinating the Zn²⁺. The same binding mode of vardenafil in PDE4B would cause steric clashes with side chains of M431^{4B} and M411^{4B}, shown in cyan, in the Q₂ pocket.

(F) Structure of vardenafil bound to PDE4B. The carbons of vardenafil bound to PDE4B are represented by cyan. In order to avoid the steric clashes with M431 and M411 in the Q₂ pocket and also the incompatible H bonding characteristics of Q443, vardenafil has flipped about 180° along the axis of C6 and N15 from its binding orientation in PDE5A. Consequently, only one H bond was formed between Q443 and the heterocyclic nitrogen in the imidazole ring. The heterocyclic nitrogen in the imidazole ring has almost traded places with the heterocyclic nitrogen in the imidazolotriazinone ring in the vardenafil bound to PDE4B as compared to the vardenafil bound to PDE5A. An H bond is formed between the exocyclic oxygen on the imidazolotriazinone ring and a water that is coordinated to the Zn²⁺.

Table 3. Data Collection, Processing, and Refinement Statistics for All the Cocrystal Structures of Various Known Inhibitors in Complex with PDE4B, PDE4D, or PDE5A

Protein Name	Inhibitor Name	Structure	D (Å)	C (%)	R _{sym}	M	R	R _{free}	Rmsd Bond (Å)	Rmsd Angle (°)	Rmsd Torsion (°)	Rama-C (%)	Rama-A (%)	Rama-G (%)	Rama-D (%)
PDE4D	zardaverine		1.54	97.8	0.065	3.4	0.178	0.195	0.007	1.115	2.735	93.60	6.40	0.00	0.00
PDE4B	(R)-rolipram		2.4	99.9	0.096	4.1	0.243	0.298	0.026	2.04	3.999	91.00	8.80	0.20	0.00
PDE4B	(R,S)-rolipram		2.31	99.4	0.091	3.8	0.205	0.25	0.017	1.591	3.242	90.30	9.50	0.20	0.00
PDE4B	filaminast		2.06	99.6	0.069	4.7	0.209	0.237	0.015	1.389	3.031	92.03	7.70	0.00	0.00
PDE4B	(R)-mesopram		1.92	100	0.067	7	0.2	0.227	0.012	1.396	3.031	92.70	7.10	0.00	0.20
PDE4B	cilomilast		2.19	93.9	0.072	4.6	0.228	0.282	0.024	1.994	3.664	91.30	8.20	0.30	0.20
PDE4D	cilomilast		1.55	99.3	0.097	3.8	0.183	0.205	0.006	1.093	2.665	92.60	7.40	0.00	0.00
PDE4B	roflumilast		2.3	91.6	0.067	4.7	0.206	0.246	0.013	1.396	2.966	91.10	8.70	0.20	0.00
PDE4D	roflumilast		1.83	97.2	0.058	3.1	0.176	0.204	0.008	1.263	2.718	93.60	6.40	0.00	0.00
PDE4B	piclamilast		2.31	98.8	0.079	4.7	0.213	0.264	0.019	1.627	3.288	92.60	7.40	0.00	0.00
PDE4D	piclamilast		1.72	97.1	0.087	3.7	0.174	0.199	0.007	1.128	2.72	93.80	6.20	0.00	0.00
PDE4B	sildenafil		2.28	99.9	0.071	5.2	0.211	0.257	0.015	1.493	5.895	90.10	9.50	0.30	0.00
PDE4B	varденаfil		2.34	99.9	0.074	4	0.21	0.259	0.018	1.703	3.292	92.00	8.00	0.00	0.00
PDE5A	varденаfil		1.79	97.6	0.058	6	0.193	0.208	0.01	1.369	2.987	93.50	6.20	0.30	0.00
PDE5A	tadalafil		1.37	96.9	0.077	3.4	0.152	0.193	0.024	1.92	4.517	94.80	5.20	0.00	0.00

(continued)

inhibitor flipping prevents possible steric clashes between the ethoxyphenyl group and M411^{4B} and M431^{4B} if the compound was to remain in the position it occupies in PDE5A. Additionally, only one H bond can now form between Q443^{4B} and sildenafil, as opposed to the two formed with Q817^{5A}. Concomitant with this loss of one H bond, the flipped orientation of sildenafil has exposed many of the hydrophobic atoms in the ethoxyphenyl group to solvent, and these two factors contributed to the significant difference in the potency of sildenafil and vardenafil toward PDE5A and PDE4B.

Conclusions

By comparing the structures of 15 inhibitor complexes across 3 members of the PDE family, we have revealed the interactions that are conserved for inhibitor binding within the PDE family as well as the regions of inhibitors that are important for selectivity toward individual PDE family members. The first conserved feature of inhibitor binding to PDEs is that the planar ring portion of the inhibitor is held tightly by a P clamp formed by highly conserved hydrophobic residues. The second conserved feature is that the inhibitor always forms one or two hydrogen bonds with the purine-selective glutamine. The P clamp provides a significant source of binding energy, while the hydrogen bond with the purine-selective glutamine affords subtype selectivity for the inhibitors. The portion of an inhibitor that forms the above-mentioned two types of interactions defines the scaffold of the inhibitor upon which potency and selectivity can be designed by adding substituents to the scaffold. The dialkoxyphenyl family of compounds can be perceived as being derived from the catechol scaffold with various substituents. These substitutions have produced compounds with increasing potency from rolipram to plicamylast. Another important feature of inhibitor binding to PDEs is that these inhibitors do not bind to the metal ions directly. Instead, they form indirect interactions with the metal ions mediated through water molecules. Therefore, hydrogen bonding to a conserved network of water molecules is likely to be an additional key feature for the design of new PDE inhibitors.

Experimental Procedures

PDE Cloning, Expression, and Purification

The cDNA encoding the catalytic domains of human PDE2A (gene number: NM_002599; coding region: H574–E941), PDE3B (NM_000922; Q650–A1084), PDE5A (NM_001083; S531–N875), PDE7B (NM_018945; Q91–P450), PDE8A (NM_02605; M1–E829), PDE9A (NM_002606; S226–A593), PDE10A (NM_006661; M432–D779), and PDE11A (NM_016953; D633–N988) were cloned into pET15S vectors (Novagen) in which a His-tag is appended to the coding sequence. The cDNA encoding the full-length human PDE8A was cloned into pFastBac vector with an N-terminal His-tag. The cloning of catalytic domains of human PDE1B, PDE4B, PDE4D, and chimeric PDE5A as well as the expres-

sion and purification of all the PDE catalytic domains were based on the protocols reported previously (Zhang et al., 2004).

Analysis of Phosphodiesterase Activity

Measurement of phosphodiesterase activity takes advantage of the selective binding of 5'-AMP or 5'-GMP (and not cAMP or cGMP) to yttrium silicate beads with embedded scintillant. Briefly, 0.1–1 nM PDE is incubated with 50 nM ³H-cAMP or 70 nM ³H-cGMP (Amersham, 5–60 Ci/mmol) in 50 mM Tris (pH 7.5), 8.3 mM MgCl₂, 1.7 mM EGTA, and 0.01% BSA at 30°C for 30 min in 384-well assay plates. The assay is terminated by adding one-third volume of 5 mg/ml yttrium silicate beads in 18 mM ZnAcetate/ZnSO₄ solution (3:1). A minimum of 30 min after mixing and centrifuging the reaction, hydrolysis is quantified by reading in a scintillation counter (Trilux, Wallac). The cAMP and cGMP concentrations used were far below the K_m of all the PDEs assayed here, except for PDE9A, in which case it is close to the K_m; thus, the IC₅₀s obtained are good approximations of K_i (Mehats et al., 2002).

Chemical Synthesis of Known PDE Inhibitors

The PDE4-specific inhibitors cilomilast (Christensen, 1993), flamlaminast (Lombardo, 1992), mesopram (Laurent et al., 1997), plicamylast (Beeley and Millican, 1993), and roflumilast (Flockerzi et al., 1995) were synthesized according to published procedures. The other PDE4-specific inhibitors, rolipram and zardaverine, were purchased from Sigma-Aldrich Corporation. The PDE5-specific inhibitors, sildenafil (Dunn and Wood, 1999), tadalafil (Daugan and Gellibert, 2000), and vardenafil (Niewohner et al., 1999), were synthesized according to published procedures.

Protein Crystallization, Data Collection, and Structure Refinement

All proteins were crystallized by using the sitting drop method. Crystals of PDE4B with various compounds were grown at 4°C by mixing equal volumes of the protein at 10 mg/ml protein with ammonium sulfate, buffered in a range of 10.0–10.5, in the presence of lithium sulfate and 1 mM compound. Crystals of PDE4D with various compounds were grown at 15°C by mixing equal volumes of the protein at 30 mg/ml with a well buffer of PEG 3350, ethylene glycol, and isopropanol, buffered in the range of 6.0–8.5 in the presence of 1 mM compound. Crystals of PDE5A chimera in complex with vardenafil and tadalafil were grown at 4°C by mixing equal volumes of the protein at 8 mg/ml with different precipitant buffers, depending on the compound used for cocrystallization, and also adding 1 mM compound. The crystallization buffer for vardenafil consists of sodium formate buffered at pH 7.0. The crystallization buffer for tadalafil consists of Jeffamine ED-2001 buffered at pH 7.0.

X-ray diffraction data were collected either at the Advanced Light Source (Lawrence Berkeley National Laboratory, Berkeley) or at Stanford Synchrotron Radiation Laboratory (Stanford Linear Accelerator Center, Menlo Park). The data were processed by Mosflm (Leslie, 1999) and Scala (Evans, 1993) driven by the ELVES (Holton and Alber, 2004) automation scripts. The cocrystal structures of PDE4B, PDE4D, and PDE5A were solved by molecular replacement by using EPMR with the PDE4B apo structure (Xu et al., 2000), the PDE4D apo structure (Huai et al., 2003c), or the PDE5A apo structure (Zhang et al., 2004) as search models, respectively. The structures were refined by CNX (Brünger et al., 1998) and REFMAC (Murshudov et al., 1999), with intermediate stages of manually rebuilding in O (Jones et al., 1991). The relevant data collection and refinement statistics are given in Table 3.

Table 3. Continued

The cocrystals of PDE4B with compounds are in the P2₁2₁2₁ space group (with the exception of sildenafil, which is in space group I2₁2₁2) and have average cell dimensions of a = 89 Å, b = 94 Å, and c = 107 Å. The crystals of PDE4D with compounds are in the P2₁2₁2₁ space group and have average cell dimensions of a = 60 Å, b = 80 Å, and c = 164 Å. The cocrystals of PDE5A with vardenafil are in space group P6₃22 with cell dimensions of a = b = 90.35 Å and c = 223.19 Å. The cocrystals of PDE5A with tadalafil are in space group C2 with cell dimensions of a = 56.10 Å, b = 76.40 Å, c = 80.70 Å, and β = 103.18°. Symbols used in the table are: D, resolution; C, completeness; M, multiplicity; R, crystallographic R factor; R_{free}, cross validation free R value; Rama-C, core region of Ramachandran plot; Rama-A, allowed region of Ramachandran plot; Rama-G, generously allowed region of Ramachandran plot; Rama-D, disallowed region of Ramachandran plot.

Acknowledgments

We thank Dr. Axel T. Brunger for critical reading of this manuscript and for discussions. We also thank our colleagues at Plexxikon for help and discussions. We thank Dr. Valsan Mandiyan, Mr. Davin Hsieh, and Ms. Hoa Nguyen for protein purification. We thank Dr. Heike Krupka, Dr. Abhinav Kumar and Dr. Weiru Wang for assisting with crystal mounting and data collection and Dr. Abhinav Kumar for assisting with structure determination. Diffraction data were collected at the Advanced Light Source and the Stanford Synchrotron Radiation Laboratory, which are supported by the U.S. Department of Energy, Office of Basic Energy Sciences under contract DE-AC03-76SF00098 and DE-AC03-76SF00515 respectively. J.S. is supported by National Institutes of Health grant 1R01-AR051448-01. All the authors except S.-H.K. and J.S. are employees of Plexxikon. S.-H.K. and J.S. are cofounders of the company and shareholders of Plexxikon stock.

Received: September 10, 2004

Revised: September 30, 2004

Accepted: October 3, 2004

Published: December 7, 2004

References

- Alvarez, R., Sette, C., Yang, D., Eglen, R.M., Wilhelm, R., Shelton, E.R., and Conti, M. (1995). Activation and selective inhibition of a cyclic AMP-specific phosphodiesterase, PDE-4D3. *Mol. Pharmacol.* **48**, 616–622.
- Ballard, S.A., Gingell, C.J., Tang, K., Turner, L.A., Price, M.E., and Naylor, A.M. (1998). Effects of sildenafil on the relaxation of human corpus cavernosum tissue in vitro and on the activities of cyclic nucleotide phosphodiesterase isozymes. *J. Urol.* **159**, 2164–2171.
- Barnette, M.S., Christensen, S.B., Essayan, D.M., Grous, M., Prabhakar, U., Rush, J.A., Kagey-Sobotka, A., and Torphy, T.J. (1998). SB 207499 (Ariflo), a potent and selective second-generation phosphodiesterase 4 inhibitor: in vitro anti-inflammatory actions. *J. Pharmacol. Exp. Ther.* **284**, 420–426.
- Beavo, J.A. (1995). Cyclic nucleotide phosphodiesterases: functional implications of multiple isoforms. *Physiol. Rev.* **75**, 725–748.
- Beavo, J.A., and Brunton, L.L. (2002). Cyclic nucleotide research—still expanding after half a century. *Nat. Rev. Mol. Cell Biol.* **3**, 710–718.
- Beeley, N.R.A., and Millican, T.A. December 1993. Trisubstituted phenyl derivatives as selective phosphodiesterase IV inhibitors. World-wide patent WO93/25517.
- Bolger, G.B., Peden, A.H., Steele, M.R., MacKenzie, C., McEwan, D.G., Wallace, D.A., Huston, E., Baillie, G.S., and Houslay, M.D. (2003). Attenuation of the activity of the cAMP-specific phosphodiesterase PDE4A5 by interaction with the immunophilin XAP2. *J. Biol. Chem.* **278**, 33351–33363.
- Brünger, A.T., Adams, P.D., Clore, G.M., DeLano, W.L., Gros, P., Grosse-Kunstleve, R.W., Jiang, J.S., Kuszewski, J., Nilges, M., Pannu, N.S., et al. (1998). Crystallography & NMR system: a new software suite for macromolecular structure determination. *Acta Crystallogr. D Biol. Crystallogr.* **54**, 905–921.
- Bundschuh, D.S., Eltze, M., Barsig, J., Wollin, L., Hatzelmann, A., and Beume, R. (2001). In vivo efficacy in airway disease models of roflumilast, a novel orally active PDE4 inhibitor. *J. Pharmacol. Exp. Ther.* **297**, 280–290.
- Burley, S.K., and Petsko, G.A. (1985). Aromatic-aromatic interaction: a mechanism of protein structure stabilization. *Science* **229**, 23–28.
- Christensen, S.B. October 1993. Compounds useful for treating allergic and inflammatory diseases. World-wide patent WO93/19479.
- Conti, M. (2000). Phosphodiesterases and cyclic nucleotide signaling in endocrine cells. *Mol. Endocrinol.* **14**, 1317–1327.
- Conti, M., and Jin, S.L. (1999). The molecular biology of cyclic nucleotide phosphodiesterases. *Prog. Nucleic Acid Res. Mol. Biol.* **63**, 1–38.
- Corbin, J.D., and Francis, S.H. (1999). Cyclic GMP phosphodiesterase-5: target of sildenafil. *J. Biol. Chem.* **274**, 13729–13732.
- Corbin, J.D., and Francis, S.H. (2002). Pharmacology of phosphodiesterase-5 inhibitors. *Int. J. Clin. Pract.* **56**, 453–459.
- Daugan, A.C., and Gellibert, F. November 2000. Tetracyclic cyclic GMP-specific phosphodiesterase inhibitors, process of preparation and use. U.S. patent 6,143,746.
- Dunn, P.J., and Wood, A.S. July 1999. Process for preparing Sildenafil. EU patent EP0812845B1.
- Evans, P.R. (1993). Data Reduction. Proceedings of CCP4 Study Weekend. On Data Collection and Processing, pp. 114–122.
- Flockerzi, D., Gutterer, B., Hatzelmann, A., Schudt, C., Beume, R., Kilian, U., and Wolf, H. January 1995. Fluoroalkoxy-substituted benzamides and their use as cyclic nucleotide phosphodiesterase inhibitors. World-wide patent WO95/01338.
- Francis, S.H., Turko, I.V., and Corbin, J.D. (2001). Cyclic nucleotide phosphodiesterases: relating structure and function. *Prog. Nucleic Acid Res. Mol. Biol.* **65**, 1–52.
- Gresser, U., and Gleiter, C.H. (2002). Erectile dysfunction: comparison of efficacy and side effects of the PDE-5 inhibitors sildenafil, vardenafil and tadalafil—review of the literature. *Eur. J. Med. Res.* **7**, 435–446.
- Hanig, H., Niewohner, U., Schenke, T., Es-Sayed, M., Schmidt, G., Lampe, T., and Bischoff, E. (2002). Imidazo[5,1-f]triazin-4(3H)-ones, a new class of potent PDE 5 inhibitors. *Bioorg. Med. Chem. Lett.* **12**, 865–868.
- Hatzelmann, A., and Schudt, C. (2001). Anti-inflammatory and immunomodulatory potential of the novel PDE4 inhibitor roflumilast in vitro. *J. Pharmacol. Exp. Ther.* **297**, 267–279.
- Holton, J., and Alber, T. (2004). Automated protein crystal structure determination using ELVES. *Proc. Natl. Acad. Sci. USA* **101**, 1537–1542.
- Houslay, M.D. (1998). Adaptation in cyclic AMP signalling processes: a central role for cyclic AMP phosphodiesterases. *Semin. Cell Dev. Biol.* **9**, 161–167.
- Houslay, M.D., and Adams, D.R. (2003). PDE4 cAMP phosphodiesterases: modular enzymes that orchestrate signalling cross-talk, desensitization and compartmentalization. *Biochem. J.* **370**, 1–18.
- Huai, Q., Colicelli, J., and Ke, H. (2003a). The crystal structure of AMP-bound PDE4 suggests a mechanism for phosphodiesterase catalysis. *Biochemistry* **42**, 13220–13226.
- Huai, Q., Liu, Y., Francis, S.H., Corbin, J.D., and Ke, H. (2003b). Crystal structures of phosphodiesterases 4 and 5 in complex with inhibitor IBMX suggest a conformation determinant of inhibitor selectivity. *J. Biol. Chem.* **279**, 13095–13101.
- Huai, Q., Wang, H., Sun, Y., Kim, H.Y., Liu, Y., and Ke, H. (2003c). Three-dimensional structures of PDE4D in complex with roliprams and implication on inhibitor selectivity. *Structure (Camb.)* **11**, 865–873.
- Huai, Q., Wang, H., Zhang, W., Colman, R.W., Robinson, H., and Ke, H. (2004). Crystal structure of phosphodiesterase 9 shows orientation variation of inhibitor 3-isobutyl-1-methylxanthine binding. *Proc. Natl. Acad. Sci. USA* **101**, 9624–9629.
- Jin, S.L., and Conti, M. (2002). Induction of the cyclic nucleotide phosphodiesterase PDE4B is essential for LPS-activated TNF- α responses. *Proc. Natl. Acad. Sci. USA* **99**, 7628–7633.
- Jones, T.A., Zou, J.Y., Cowan, S.W., and Kjeldgaard, M. (1991). Improved methods for building protein models in electron density maps and the location of errors in these models. *Acta Crystallogr. A* **47**, 110–119.
- Laurent, H., Ottow, E., Kirsch, G., Wachtel, H., Schneider, H., Faulds, D., and Dinter, H. May 1997. Chiral methylphenyl oxazolidinones. World-wide patent WO97/15561.
- Lee, M.E., Markowitz, J., Lee, J.O., and Lee, H. (2002). Crystal structure of phosphodiesterase 4D and inhibitor complex. *FEBS Lett.* **530**, 53–58.
- Leslie, A.G. (1999). Integration of macromolecular diffraction data. *Acta Crystallogr. D Biol. Crystallogr.* **55**, 1696–1702.

Lombardo, L.J. June 1992. Oxime-carbamates and oxime-carbonates as bronchodilators and anti-inflammatory agents. U.S. patent 5,124,455.

McPhee, I., Yarwood, S.J., Scotland, G., Huston, E., Beard, M.B., Ross, A.H., Houslay, E.S., and Houslay, M.D. (1999). Association with the SRC family tyrosyl kinase LYN triggers a conformational change in the catalytic region of human cAMP-specific phosphodiesterase HSPDE4A4B. Consequences for rolipram inhibition. *J. Biol. Chem.* 274, 11796–11810.

Mehats, C., Andersen, C.B., Filopanti, M., Jin, S.L., and Conti, M. (2002). Cyclic nucleotide phosphodiesterases and their role in endocrine cell signaling. *Trends Endocrinol. Metab.* 13, 29–35.

Murshudov, G.N., Vagin, A.A., Lebedev, A., Wilson, K.S., and Dodson, E.J. (1999). Efficient anisotropic refinement of macromolecular structures using FFT. *Acta Crystallogr. D Biol. Crystallogr.* 55, 247–255.

Niewohner, U., Es-Sayed, M., Haning, H., Schenke, T., Schlemmer, K.H., Keldenich, J., Bischoff, E., Perzborn, E., Dembowski, K., Serno, P., and Nowakowski, M. May 1999. 2-Phenyl-substituted imidazotriazinones as phosphodiesterase inhibitors. World-wide patent WO99/24433.

Porst, H. (2002). IC351 (tadalafil, Cialis): update on clinical experience. *Int. J. Impot. Res.* 14, S57–S64.

Robichaud, A., Stamatiou, P.B., Jin, S.L., Lachance, N., MacDonald, D., Laliberte, F., Liu, S., Huang, Z., Conti, M., and Chan, C.C. (2002). Deletion of phosphodiesterase 4D in mice shortens alpha(2)-adrenoceptor-mediated anesthesia, a behavioral correlate of emesis. *J. Clin. Invest.* 110, 1045–1052.

Rocque, W.J., Tian, G., Wiseman, J.S., Holmes, W.D., Zajac-Thompson, I., Willard, D.H., Patel, I.R., Wisely, G.B., Clay, W.C., Kadwell, S.H., et al. (1997). Human recombinant phosphodiesterase 4B2B binds (R)-rolipram at a single site with two affinities. *Biochemistry* 36, 14250–14261.

Rotella, D.P. (2002). Phosphodiesterase 5 inhibitors: current status and potential applications. *Nat. Rev. Drug Discov.* 1, 674–682.

Scapin, G., Patel, S.B., Chung, C., Varnerin, J.P., Edmondson, S.D., Mastracchio, A., Parmee, E.R., Singh, S.B., Becker, J.W., Van Der Ploeg, L.H., et al. (2004). Crystal structure of human phosphodiesterase 3B: atomic basis for substrate and inhibitor specificity. *Biochemistry* 43, 6091–6100.

Schudt, C., Winder, S., Muller, B., and Ukena, D. (1991). Zardaverine as a selective inhibitor of phosphodiesterase isozymes. *Biochem. Pharmacol.* 42, 153–162.

Souness, J.E., Aldous, D., and Sargent, C. (2000). Immunosuppressive and anti-inflammatory effects of cyclic AMP phosphodiesterase (PDE) type 4 inhibitors. *Immunopharmacology* 47, 127–162.

Sung, B.J., Yeon Hwang, K., Ho Jeon, Y., Lee, J.I., Heo, Y.S., Hwan Kim, J., Moon, J., Min Yoon, J., Hyun, Y.L., Kim, E., et al. (2003). Structure of the catalytic domain of human phosphodiesterase 5 with bound drug molecules. *Nature* 425, 98–102.

Terry, R., Cheung, Y.F., Praestegaard, M., Baillie, G.S., Huston, E., Gall, I., Adams, D.R., and Houslay, M.D. (2003). Occupancy of the catalytic site of the PDE4A4 cyclic AMP phosphodiesterase by rolipram triggers the dynamic redistribution of this specific isoform in living cells through a cyclic AMP independent process. *Cell. Signal.* 15, 955–971.

Xu, R.X., Hassell, A.M., Vanderwall, D., Lambert, M.H., Holmes, W.D., Luther, M.A., Rocque, W.J., Milburn, M.V., Zhao, Y., Ke, H., and Nolte, R.T. (2000). Atomic structure of PDE4: insights into phosphodiesterase mechanism and specificity. *Science* 288, 1822–1825.

Xu, R.X., Rocque, W.J., Lambert, M.H., Vanderwall, D.E., Luther, M.A., and Nolte, R.T. (2004). Crystal structures of the catalytic domain of phosphodiesterase 4B complexed with amp 8-br-AMP, and rolipram. *J. Mol. Biol.* 337, 355–365.

Zhang, K.Y.J., Card, G.L., Suzuki, Y., Artis, D.R., Fong, D., Gillette, S., Hsieh, D., Neiman, J., West, B.L., Zhang, C., et al. (2004). A glutamine switch mechanism for nucleotide selectivity by phosphodiesterases. *Mol. Cell* 15, 279–286.

Accession Numbers

The coordinates and structure factors of the cocrystal structures have been deposited in the Protein Data Bank with the accession number 1XLX for cilomilast with PDE4B, 1XLZ for filaminast with PDE4B, 1XM6 for (R)-mesopram with PDE4B, 1XM4 for piclamilast with PDE4B, 1XMU for roflumilast with PDE4B, 1XMY for (R)-rolipram with PDE4B, 1XN0 for (R,S)-rolipram with PDE4B, 1XOS for sildenafil with PDE4B, 1XOT for vardenafil with PDE4B, 1XOM for cilomilast with PDE4D, 1XON for piclamilast with PDE4D, 1XOQ for roflumilast with PDE4D, 1XOR for zardaverine with PDE4D, 1XOZ for tadalafil with PDE5A, and 1XP0 for vardenafil with PDE5A.